## Genuinely Multidimensional Upwinding for the 2D Shallow Water Equations <sup>1</sup>

P. Garcia-Navarro<sup>2</sup>, M. E. Hubbard and A. Priestley
Dept. of Mathematics,
P.O. Box 220,
University of Reading,
Whiteknights,
Reading,
U.K.

<sup>&</sup>lt;sup>1</sup>The first author was funded by the EC Program of Human Capital and Mobility, the second by DRA Farnborough and the third by the U.K. S.E.R.C.

<sup>&</sup>lt;sup>2</sup>on leave from the University of Zaragoza

## Abstract

A multidimensional upwinding technique is applied to the simulation of 2D shallow water flows. It is adapted from fluctuation splitting methods recently proposed for the solution of the Euler system of equations on unstructured triangular grids. The basis of the numerical method is stated and the particular adaptation to the shallow water system is described. Numerical results of interest to hydraulic engineers are presented. Despite the complexities of the scheme advantages related to the use of a discretisation based on triangles would seem to make the schemes competitive with those currently in use.

## 1 Introduction

In reading the literature of recent years on the latest advances in numerical methods for hyperbolic conservation laws, one might gain the impression that many more people worked on problems involving the Euler equations than on problems concerning the shallow water equations. In practice, though, this is not the situation, with many more engineers, physicists and mathematicians being involved in solving problems of the latter kind on a day to day basis.

Classical methods and central difference schemes still dominate the commercial software products for this market, with Preissmann's, Abbott's (see [4] for example) and McCormack's [7] schemes the most commonly used. These schemes are well known to require special treatment in many situations so that the calculations may proceed.

Some years after their adoption for solving problems in gas dynamics, upwind and TVD (Total Variation Diminishing) numerical schemes have been successfully used for the solution of the shallow water equations, with similar advantages [8]. Their use is nevertheless only gradually gaining acceptance in this sector.

Recently, in the context of gas dynamics, doubt has been expressed as to whether the essentially 1D TVD schemes are the most suitable choice for multi-dimensional calculations, and the search has been initiated for genuinely multi-dimensional approaches. Most of these are based on piecewise constant representations of the solution on triangular grids with a 1D upwinding of the Riemann problem for each edge of the triangle. However, it has been claimed that such an approach is weak when the solution is not constant along a triangle edge, since it may misinterpret features which are not aligned with grid interfaces.

In a different philosophy, instead of concentrating on finite volumes and the changes of the variables across the cell sides, Deconinck et al. [5] consider solutions on triangular grids in which the unknowns are associated with the vertices and updates to these nodal values are through the advection of linear wave solutions. This avoids the problems of taking the normal to the cell interfaces as a privileged direction.

Reference [5] is concerned with gas dynamics applications. In this paper we consider the use of this technique for 2D shallow water flows and the question of whether they may be of practical use. In the next sections, the basis of the numerical method is stated and the adaptation to the shallow water system is described. The numerical treatment of the boundaries as well as the inclusion of source terms in the governing equations are also discussed. Finally, some numerical results are presented. Although this work is at an early stage, our results indicate that the advantages may outweigh the disadvantages and that these schemes may have a future for hydraulic engineering applications.

## 2 Basic Technique

#### 2.1 Scalar case

For the numerical solution of the 2D linear scalar equation

$$\frac{\partial w}{\partial t} + \mathbf{a} \cdot \nabla w = 0 \quad , \quad \mathbf{a} = (a_x, a_y) \tag{2.1}$$

with constant  $\mathbf{a}$ , we assume the given physical domain to be discretised by triangular cells and a set of initial values  $w_i$  stored at the nodes of the mesh. For each cell T, of area  $S_T$ , a cell fluctuation is defined as

$$\Phi_T = \int_T \frac{\partial w}{\partial t} dS \tag{2.2}$$

and a cell residual  $R_T$  as

$$R_T = -\frac{1}{S_T} \Phi_T = \frac{1}{S_T} \int_T \mathbf{a} \cdot \nabla w dS = -\frac{1}{S_T} \oint_C w \mathbf{a} \cdot \mathbf{n} dC$$
 (2.3)

where C represents the cell boundary and  $\mathbf{n}$  is the inward unit normal to the cell boundary. The cell fluctuation or cell residual contains information on the state of the cell to be transmitted to w over a time step, so that the changes made to the values of the  $w_i$ 's at the nodes of triangle T will be proportional to  $\Phi_T$  or  $R_T$ . The distribution of the information to the nodes should, if possible, be done in a way which ensures conservation [15].

From the properties of the normals in the cell and the additional assumption that the solution varies linearly within each element, it is possible to identify a discrete approximation of  $\nabla w$ , where  $\mathbf{n}_i$  is the normal to the edge opposite node i,

$$\nabla w_T = \frac{1}{2S_T} \sum_{i=1}^3 w_i \mathbf{n}_i \tag{2.4}$$

such that

$$R_T = \mathbf{a} \cdot \nabla w_T, \tag{2.5}$$

or

$$\Phi_T = -\sum_{i=1}^3 w_i k_i \tag{2.6}$$

with the introduction of the quantities

$$k_i = \frac{1}{2} \mathbf{a} \cdot \mathbf{n}_i \tag{2.7}$$

which contain information about the direction of advection relative to the cell. They can be used to decide whether flow enters or leaves the triangle through a particular edge and, in that sense, are a useful tool for the upwind properties of the technique.

Residuals and fluctuations are cell-based quantities which are going to be used for the updating of the nodal values. For this purpose we introduce distribution coefficients,  $D_T^i$ , defining the weightings of the residual to the nodes in a cell. For conservation and consistency they must satisfy

$$\sum_{i=1}^{3} D_T^i = 1$$

in every cell, see [5] for example. Then, a first order explicit time-stepping procedure at the nodes can be defined as

$$w_i^{n+1} = w_i^n - \frac{\Delta t}{S_i} \left[ \sum_{T_i} S_T D_T^i R_T^n \right],$$
 (2.8)

where the sum is over all the cells meeting at node i, and where  $S_i = \frac{1}{3} \sum_{T_i} S_T$ . In order to focus on the individual cell treatment, the advection scheme can be expressed, on each triangle, as

$$S_{1}w_{1}^{n+1} = S_{1}w_{1}^{n} - \Delta t S_{T}D_{T}^{1}R_{T}^{n}$$

$$S_{2}w_{2}^{n+1} = S_{2}w_{2}^{n} - \Delta t S_{T}D_{T}^{2}R_{T}^{n}$$

$$S_{3}w_{3}^{n+1} = S_{3}w_{3}^{n} - \Delta t S_{T}D_{T}^{3}R_{T}^{n},$$

$$(2.9)$$

where only the influence from the individual triangle has been included.

There exist many criteria for the design of advection schemes, depending on the choice of the distribution coefficients. Two properties are of interest, positivity and linearity preservation of the scheme. The former is related to the 1D property of monotonicity whilst the second has to do with the accuracy of the method. Unfortunately, their simultaneous requirement is incompatible with the linearity of a scheme. This leads to the generation of non-linear advection schemes, even for linear equations. These schemes are based on the construction of advection speed vectors  $\mathbf{a}_m$  in the direction of the local gradient, defined as

$$\mathbf{a}_m = a_m \mathbf{m}$$

with

$$\mathbf{m} = \frac{\nabla w}{|\nabla w|}$$
 and  $a_m = \mathbf{a} \cdot \mathbf{m}$ .

This makes the coefficients  $k_i$  of (2.7) dependent on the solution, enabling the simultaneous satisfaction of the two desired properties. Note that the use of the frontal speed  $\mathbf{a}_m$  does not alter the cell residual, since

$$\mathbf{a} \cdot \nabla w = \mathbf{a}_m \cdot \nabla w.$$

If the equation to be solved is non-linear, a suitable linearization must be performed before the techniques described for the linear equation are applied. Given the non-linear equation

$$\frac{\partial w}{\partial t} + \nabla \cdot \mathbf{F}(w) = 0$$
 ,  $\mathbf{F} = (F, G)$ 

where

$$\mathbf{a} = (F_w, G_w),$$

the fluctuation is defined as

$$\Phi_T = -\int_T \nabla . \mathbf{F} dS.$$

An averaged advection speed which satisfies discrete conservation can now be found by assuming linear variation of w over the cell and therefore constant gradient  $\nabla w$ . In that case

$$\int_{T} \nabla \cdot \mathbf{F} dS = \int_{T} (F_x + G_y) dS = \int_{T} (F_w w_x + G_w w_y) dS$$
$$= w_x \int_{T} F_w dS + w_y \int_{T} G_w dS = (\bar{a}_x w_x + \bar{a}_y w_y) S_T$$

where

$$\bar{a}_x = \frac{1}{S_T} \int_T F_w dS \; , \; \bar{a}_y = \frac{1}{S_T} \int_T G_w dS,$$

and

$$\Phi_T = -S_T \bar{\mathbf{a}} \cdot \nabla w \ , \ k_i = \frac{1}{2} \bar{\mathbf{a}} \cdot \bar{\mathbf{n}}_i,$$

with

$$\bar{\mathbf{a}} = (\bar{a}_x, \bar{a}_y)$$

Since the advection schemes used for the shallow water equations are no different for those used for the Euler equations we will not go into further detail about their particular construction and description. We refer the reader to the very good reviews in [10] and [15].

#### 2.2 Systems of equations

The application of multi-dimensional upwinding to a general non-linear 2D system of conservation laws

$$\frac{\partial \mathbf{w}}{\partial t} + \nabla \cdot (\mathbf{F}(\mathbf{w})) = 0$$
 ,  $\mathbf{F} = (\mathbf{f}, \mathbf{g})$ 

requires a discrete form, for the conserved variables  $\mathbf{w}$ , of the linearization

$$\frac{\partial \mathbf{w}}{\partial t} + (A, B)\nabla(\mathbf{w}) = 0.$$

Where, in particular, a consistent approximation for the cell residual is sought

$$\mathbf{R}_T = (\bar{A}, \bar{B})_T \cdot \nabla \mathbf{w}_T \tag{2.10}$$

where  $\bar{A}_T$ ,  $\bar{B}_T$  are discrete equivalents of the cell averaged Jacobian matrices, calculated using the nodal values. The assumption of linear variation of  $\mathbf{w}$  on each cell, enables us to write

$$\mathbf{R}_{T} = \frac{1}{S_{T}} \int_{T} (A, ) \cdot \nabla \mathbf{w} dS$$

$$= \frac{1}{S_{T}} \nabla \mathbf{w}_{T} \int_{T} (A, B) dS$$
(2.11)

where discrete cell gradients and cell Jacobians can be defined in the same form as for the scalar case

$$\nabla \mathbf{w}_{T} = \frac{1}{S_{T}} \sum_{i=1}^{3} \mathbf{w}_{i} \mathbf{n}_{i}$$

$$\bar{A} = \frac{1}{S_{T}} \int_{T} A dS$$

$$\bar{B} = \frac{1}{S_{T}} \int_{T} B dS$$

Unfortunately, the exact evaluation of the above integrals is not practical either for the Euler or for the shallow water equations. Roe [13] suggested the introduction of a parameter set of variables for a simpler treatment of the former system. The strategy we have followed for the shallow water equations makes use of the set of primitive variables and is described in the next section.

### 3 The 2D Shallow Water System

We begin this section by writing the homogeneous version of the system of equations in terms of the conserved variables,

$$\mathbf{U} = (h , uh , vh)^T, \tag{3.1}$$

where h, u and v are the depth and x and y velocities respectively, that is,

$$\frac{\partial \mathbf{U}}{\partial t} + \frac{\partial \mathbf{E}}{\partial x} + \frac{\partial \mathbf{F}}{\partial y} = 0 \tag{3.2}$$

where the fluxes are,

$$\mathbf{E} = \begin{pmatrix} uh \\ u^2h + \frac{gh^2}{2} \\ uvh \end{pmatrix} , \quad \mathbf{F} = \begin{pmatrix} vh \\ uvh \\ v^2h + \frac{gh^2}{2} \end{pmatrix}.$$

It can be rewritten in terms of the same variables but in a non-conservative form as,

$$\frac{\partial \mathbf{U}}{\partial t} + A \frac{\partial \mathbf{U}}{\partial x} + B \frac{\partial \mathbf{U}}{\partial y} = 0 \tag{3.3}$$

in which the two Jacobian matrices are

$$A = \frac{\partial \mathbf{E}}{\partial \mathbf{U}} = \begin{pmatrix} 0 & 1 & 0 \\ -u^2 + gh & 2u & 0 \\ -uv & v & u \end{pmatrix} , B = \frac{\partial \mathbf{F}}{\partial \mathbf{U}} = \begin{pmatrix} 0 & 0 & 1 \\ -uv & v & u \\ -v^2 + gh & 0 & 2v \end{pmatrix}.$$

As mentioned earlier, it will be useful later on in the paper to express the equations in terms of the primitive variables

$$\mathbf{V} = (h , u , v)^T \tag{3.4}$$

in a non-conservative way, as follows,

$$\frac{\partial \mathbf{V}}{\partial t} + G \frac{\partial \mathbf{V}}{\partial x} + H \frac{\partial \mathbf{V}}{\partial y} = 0, \tag{3.5}$$

where the new matrices G and H are,

$$G = \left(\begin{array}{ccc} u & h & 0 \\ g & u & 0 \\ 0 & 0 & u \end{array}\right) \ , \ H = \left(\begin{array}{ccc} v & 0 & h \\ 0 & v & 0 \\ g & 0 & v \end{array}\right).$$

It is worth noting that the transformation matrix, M, has the form

$$M = \frac{\partial \mathbf{U}}{\partial \mathbf{V}} = \begin{pmatrix} 1 & 0 & 0 \\ u & h & 0 \\ v & 0 & h \end{pmatrix}.$$

In the conservative formulation, the fluctuation is defined as

$$\Phi_T = \int_T \mathbf{U}_t dS = -\int_T (\mathbf{E}_x + \mathbf{F}_y) dS.$$
 (3.6)

We can use the relation between the two sets of variables to define new matrices R and S,

$$R = \frac{\partial \mathbf{E}}{\partial \mathbf{V}} = \frac{\partial \mathbf{E}}{\partial \mathbf{U}} \frac{\partial \mathbf{U}}{\partial \mathbf{V}} = AM$$
$$S = \frac{\partial \mathbf{F}}{\partial \mathbf{V}} = \frac{\partial \mathbf{F}}{\partial \mathbf{U}} \frac{\partial \mathbf{U}}{\partial \mathbf{V}} = BM$$

so that:

$$\mathbf{E}_x + \mathbf{F}_y = \mathbf{E}_V \mathbf{V}_x + \mathbf{F}_V \mathbf{V}_y = R \mathbf{V}_x + S \mathbf{V}_y.$$

Provided that the variables V are linear over the cells T, the gradients,  $V_x$  and  $V_y$ , are constant, and this enables us to write the fluctuation as

$$\Phi_{T} = -\left(\int_{T} (R(\mathbf{V})\mathbf{V}_{x} + S(\mathbf{V})\mathbf{V}_{y})dS \right)$$

$$= -\left(\int_{T} (R(\mathbf{V})dS)\mathbf{V}_{x} - \left(\int_{T} (S(\mathbf{V})dS)\mathbf{V}_{y}\right)\right)$$

$$= -S_{T}[\bar{R}\mathbf{V}_{x} + \bar{S}\mathbf{V}_{y}] \tag{3.7}$$

with the definitions:

$$\bar{R} = \frac{1}{S_T} \int_T R(\mathbf{V}) dS , \ \bar{S} = \frac{1}{S_T} \int_T S(\mathbf{V}) dS.$$
 (3.8)

We now replace  $\bar{R}$ ,  $\bar{S}$  by

$$\bar{R} = R(\bar{\mathbf{V}}) , \ \bar{S} = S(\bar{\mathbf{V}})$$
 (3.9)

where the averaged variables are simply

$$\bar{\mathbf{V}} = \begin{pmatrix} \bar{h} \\ \bar{u} \\ \bar{v} \end{pmatrix} = \frac{1}{3} \begin{pmatrix} h_1 + h_2 + h_3 \\ u_1 + u_2 + u_3 \\ v_1 + v_2 + v_3 \end{pmatrix}$$
(3.10)

summing over the nodal values at the vertices of the triangle T. Note that with this definition of  $\bar{R}$ ,  $\bar{S}$  we are only approximating equation (3.8), unlike in the Euler equations where an exact representation of the integral is obtained because in this case R is linear in  $\mathbf{V}$ .

We are seeking a conservative discrete approximation of the Jacobians satisfying

$$(\Phi_T \approx) - S_T(\bar{\mathbf{E}}_x + \bar{\mathbf{F}}_y) = -S_T(\bar{A}\bar{\mathbf{U}}_x + \bar{B}\bar{\mathbf{U}}_y). \tag{3.11}$$

From (3.7) it is easy to identify

$$\begin{aligned}
\bar{\mathbf{E}}_x &= \bar{R}\mathbf{V}_x \\
\bar{\mathbf{F}}_y &= \bar{S}\mathbf{V}_y.
\end{aligned} (3.12)$$

Moreover, we can use the change of variables to define

$$S_T \bar{\mathbf{U}}_x = \int_T \mathbf{U}_x dS = \int_T M(\mathbf{V}) \mathbf{V}_x dS = S_T M(\bar{\mathbf{V}}) \mathbf{V}_x$$

so that

$$\bar{\mathbf{U}}_r = M(\bar{\mathbf{V}})\mathbf{V}_r \tag{3.13}$$

$$\mathbf{V}_{r} = M^{-1}(\bar{\mathbf{V}})\bar{\mathbf{U}}_{r} \tag{3.14}$$

with similar expressions for  $\bar{\mathbf{U}}_y$  and  $\mathbf{V}_y$ . This can be used to rewrite the fluctuation in terms of suitable averages of the conserved variables,

$$(\Phi_T \approx) -[\bar{R}M^{-1}(\bar{\mathbf{V}})\bar{\mathbf{U}}_x + \bar{S}M^{-1}(\bar{\mathbf{V}})\bar{\mathbf{U}}_y]S_T$$
  
=  $-[\bar{A}\bar{\mathbf{U}}_x + \bar{B}\bar{\mathbf{U}}_y]S_T,$  (3.15)

which allows the identification of  $\bar{A}$  and  $\bar{B}$ .

$$\bar{A} = R(\bar{\mathbf{V}})M^{-1}(\bar{\mathbf{V}}) = \frac{\partial \mathbf{E}}{\partial \mathbf{V}} \Big|_{\bar{V}} \frac{\partial \mathbf{V}}{\partial \mathbf{U}} \Big|_{\bar{V}} = \frac{\partial \mathbf{E}}{\partial \mathbf{U}} \Big|_{\bar{V}} = A(\bar{V})$$

$$\bar{B} = S(\bar{\mathbf{V}})M^{-1}(\bar{\mathbf{V}}) = \frac{\partial \mathbf{F}}{\partial \mathbf{V}} \Big|_{\bar{V}} \frac{\partial \mathbf{V}}{\partial \mathbf{U}} \Big|_{\bar{V}} = \frac{\partial \mathbf{F}}{\partial \mathbf{U}} \Big|_{\bar{V}} = B(\bar{V}) \tag{3.16}$$

The next thing we have to do is to compute the residuals  $R_T$  or the fluctuations and distribute them to the vertices of every cell by means of an advection scheme. Recalling that at the beginning of the time step we have the values of the conserved variables at the vertices of the triangular mesh, the steps to follow are: to compute the primitive variables  $\mathbf{V}$  from the known  $\mathbf{U}$ , work out the gradients  $\nabla \mathbf{V} = (\mathbf{V}_x, \mathbf{V}_y)$  within each triangle, and decompose the residual into parts that can be explained as due to the passage of a wave. The latter step will require a description of wave models.

#### 4 Wave Models

Consider the linearized system of equations written in primitive variables

$$\frac{\partial \mathbf{V}}{\partial t} + \bar{G}\frac{\partial \mathbf{V}}{\partial x} + \bar{H}\frac{\partial \mathbf{V}}{\partial y} = 0. \tag{4.1}$$

A simple wave solution can be found, as in Roe [11,12], in the form

$$\mathbf{V} = \mathbf{V}(\xi)$$
 with  $\xi = \mathbf{x}.\mathbf{n}_{\theta} - \lambda_{\theta}t$ 

where  $\mathbf{n}_{\theta} = (\cos \theta, \sin \theta)$  gives the direction of propagation and  $\lambda_{\theta}$  the speed of the wave. If we note that

$$\frac{\partial \mathbf{V}}{\partial t} = -\lambda_{\theta} \frac{d\mathbf{V}}{d\xi}$$

 $\quad \text{and} \quad$ 

$$\nabla \mathbf{V} = \frac{d\mathbf{V}}{d\xi} \mathbf{n}_{\theta},$$

it follows from (4.1) that

$$-\lambda_{\theta} \frac{d\mathbf{V}}{d\xi} + (\bar{G}cos\theta + \bar{H}sin\theta)\frac{d\mathbf{V}}{d\xi} = 0$$

which means that  $\frac{d\mathbf{V}}{d\xi}$  are the right eigenvectors of the matrix

$$M^* = \bar{G}\cos\theta + \bar{H}\sin\theta \tag{4.2}$$

and  $\lambda_{\theta}$  the corresponding eigenvalues.

It is then possible to express the gradient as the sum

$$\nabla \mathbf{V} = \sum_{k=1}^{n} \alpha^k \mathbf{r}^k \mathbf{n}^k \tag{4.3}$$

that is,

$$\mathbf{V}_x = \sum_{k=1}^n \alpha^k \mathbf{r}^k \cos \theta^k$$

$$\mathbf{V}_y = \sum_{k=1}^n \alpha^k \mathbf{r}^k \sin \theta^k.$$

The vectors  $\mathbf{r}^k$  are the right eigenvectors of the matrix  $M^*$ :

$$\mathbf{r}^{1} = \begin{pmatrix} 1 \\ \frac{g}{c}cos\theta \\ \frac{g}{c}sin\theta \end{pmatrix}, \quad \mathbf{r}^{2} = \begin{pmatrix} 1 \\ -\frac{g}{c}cos\theta \\ -\frac{g}{c}sin\theta \end{pmatrix}, \quad \mathbf{r}^{n} = \begin{pmatrix} 0 \\ -sin\theta \\ cos\theta \end{pmatrix}. \tag{4.4}$$

The variables  $\alpha^k$  represent weighting coefficients of the sum and  $\theta^k$  are the different angles of each wave. The celerity, c, is the equivalent of the speed of sound in gas-dynamics and is the velocity of small perturbations in still water, given by  $c = \sqrt{gh}$ .

The connection expressed in (3.13) between the gradient of the primitive variables and that of the averaged conservative variables can be used to develop the latter as

$$\bar{\mathbf{U}}_x = \sum_{k=1}^n \alpha^k \mathbf{r}_c^k cos \theta^k$$

$$\bar{\mathbf{U}}_y = \sum_{k=1}^n \alpha^k \mathbf{r}_c^k \sin \theta^k$$

where now,  $\mathbf{r}_c^k$  represent the right eigenvectors of the matrix

$$M_c^* = \bar{A}cos\theta + \bar{B}sin\theta$$

and can be worked out through  $\mathbf{r}_c^k = M(\bar{\mathbf{V}})\mathbf{r}^k$ . It is worth noting here that the two matrices  $M^*$  and  $M_c^*$  share the unique set of eigenvalues,  $\lambda^k$ ,

$$\lambda^{1} = \bar{u}\cos\theta + \bar{v}\sin\theta + c$$

$$\lambda^{2} = \bar{u}\cos\theta + \bar{v}\sin\theta - c$$

$$\lambda^{3} = \bar{u}\cos\theta + \bar{v}\sin\theta.$$
(4.5)

The residual then can be split into a sum of waves

$$R_{T} = \bar{A}\bar{\mathbf{U}}_{x} + \bar{B}\bar{\mathbf{U}}_{y}$$

$$= \bar{A}\sum_{k=1}^{n} \alpha^{k}\mathbf{r}_{c}^{k}\cos\theta^{k} + \bar{B}\sum_{k=1}^{n} \alpha^{k}\mathbf{r}_{c}^{k}\sin\theta^{k}$$

$$= \sum_{k=1}^{n} \alpha^{k}[\bar{A}\cos\theta^{k} + \bar{B}\sin\theta^{k}]\mathbf{r}_{c}^{k}$$

$$= \sum_{k=1}^{n} \alpha^{k}\lambda^{k}\mathbf{r}_{c}^{k}.$$

$$(4.6)$$

We next describe two of the several wave models proposed in the literature to accomplish the above decomposition.

#### 4.1 Roe's wave models

The wave decomposition of the gradient of the primitive variables, namely,

$$\nabla \mathbf{V} = \sum_{k=1}^{n} \alpha^k \mathbf{r}^k \mathbf{n}^k, \tag{4.7}$$

represents a system of 6 equations in the shallow water case, where we have two spatial derivatives for each of the three variables. Therefore, it allows for 6 unknowns. These must correspond to either the coefficients or angles of a propagation of suitable choices of waves whose advection will represent the total fluctuation.

Following Roe's suggestions for the treatment of the Euler equations [11], the splitting can be made into four orthogonal acoustic waves, labelled by their strengths (coefficients) and one angle  $\theta$  which determines the four directions, defined by

$$(\alpha_1 , \theta), (\alpha_2 , \theta + \pi), (\alpha_3 , \theta + \frac{\pi}{2}), (\alpha_4 , \theta + \frac{3\pi}{2}),$$

as well as one shear wave  $(\beta, \phi)$  of strength  $\beta$  at an angle  $\phi$ . The six unknowns are then  $\alpha_1, \alpha_2, \alpha_3, \alpha_4, \beta$  and  $\theta$ . The value of the angle  $\phi$ , in Roe's model D, can

be defined in terms of the solution as

$$\phi = \theta - \frac{\pi}{4} sign(\beta).$$

Making use of the equivalences of the basic trigonometric functions to those of the first quadrant of the unit radius circle, the system (4.7) can be explicitly written as follows:

$$\frac{\partial h}{\partial x} = \alpha_1 \cos\theta - \alpha_2 \cos\theta - \alpha_3 \sin\theta + \alpha_4 \sin\theta 
\frac{\partial h}{\partial y} = \alpha_1 \sin\theta - \alpha_2 \sin\theta + \alpha_3 \cos\theta - \alpha_4 \cos\theta 
\frac{\partial u}{\partial x} = \frac{g}{c} [\alpha_1 \cos^2\theta + \alpha_2 \cos^2\theta + \alpha_3 \sin^2\theta + \alpha_4 \sin^2\theta] - \beta \sin\phi \cos\phi 
\frac{\partial u}{\partial y} = \frac{g}{c} [\alpha_1 \sin\theta \cos\theta + \alpha_2 \sin\theta \cos\theta - \alpha_3 \sin\theta \cos\theta - \alpha_4 \sin\theta \cos\theta] - \beta \sin^2\phi 
\frac{\partial v}{\partial x} = \frac{g}{c} [\alpha_1 \sin\theta \cos\theta + \alpha_2 \sin\theta \cos\theta - \alpha_3 \sin\theta \cos\theta - \alpha_4 \sin\theta \cos\theta] + \beta \cos^2\phi 
\frac{\partial v}{\partial y} = \frac{g}{c} [\alpha_1 \sin^2\theta + \alpha_2 \sin^2\theta + \alpha_3 \cos^2\theta + \alpha_4 \cos^2\theta] + \beta \sin\phi \cos\phi.$$
(4.8)

The solution of the above algebraic system is easily found giving, for the coefficient of the shear wave,

$$\beta = |\beta| \operatorname{sign}(\beta) = v_x - u_y. \tag{4.9}$$

The identities

$$\beta(\cos^2\phi - \sin^2\phi) = |\beta| \sin 2\theta$$
$$2\beta \sin\phi \cos\phi = -|\beta| \cos 2\theta$$

are helpful in combining the derivatives as

$$u_y + v_x = \left[\frac{g}{c}(\alpha_1 + \alpha_2 - \alpha_3 - \alpha_4) + |\beta|\right] \sin 2\theta$$
$$u_x - v_y = \left[\frac{g}{c}(\alpha_1 + \alpha_2 - \alpha_3 - \alpha_4) + |\beta|\right] \cos 2\theta$$

so that

$$tan2\theta = \frac{u_y + v_x}{u_x - v_y}. (4.10)$$

Further manipulations of the derivatives lead us to

$$u_x \cos^2 \theta - v_y \sin^2 \theta = \left[\frac{g}{c}(\alpha_1 + \alpha_2) + \frac{1}{2}|\beta|\right] \cos 2\theta$$

 $\quad \text{and} \quad$ 

$$h_x cos\theta + h_y sin\theta = \alpha_1 - \alpha_2,$$

hence, to the values

$$\alpha_1 = \frac{1}{2} \left[ h_x \cos\theta + h_y \sin\theta + \frac{c}{g} \left( \frac{u_x \cos^2\theta - v_y \sin^2\theta}{\cos 2\theta} - \frac{1}{2} |\beta| \right) \right]$$
(4.11)

$$\alpha_2 = \frac{1}{2} \left[ -(h_x cos\theta + h_y sin\theta) + \frac{c}{g} \left( \frac{u_x cos^2\theta - v_y sin^2\theta}{cos2\theta} - \frac{1}{2} |\beta| \right) \right].$$
 (4.12)

A similar procedure gives

$$\alpha_3 = \frac{1}{2} \left[ h_y \cos\theta - h_x \sin\theta + \frac{c}{q} \left( \frac{v_y \cos^2\theta - u_x \sin^2\theta}{\cos^2\theta} + \frac{1}{2} |\beta| \right) \right]$$
(4.13)

$$\alpha_4 = \frac{1}{2} \left[ -(h_y cos\theta - h_x sin\theta) + \frac{c}{g} \left( \frac{v_y cos^2\theta - u_x sin^2\theta}{cos2\theta} + \frac{1}{2} |\beta| \right) \right]. \quad (4.14)$$

#### 4.2 Rudgyard's wave models

These are mainly based on the idea of obtaining the six waves by choosing two, in principle, arbitrary propagation angles,  $\theta_1$  and  $\theta_2$ , and performing a decomposition of the gradient,

$$\nabla \mathbf{V} = \sum_{k=1}^{3} \alpha_{\theta 1}^{k} \mathbf{r}_{\theta 1}^{k} \mathbf{n}_{\theta 1} + \sum_{k=1}^{3} \alpha_{\theta 2}^{k} \mathbf{r}_{\theta 2}^{k} \mathbf{n}_{\theta 2}$$
(4.15)

which contains six free parameters, the six  $\alpha$  coefficients. The vectors  $\mathbf{n}_{\theta} = (\cos\theta, \sin\theta)$  are again the unit vectors in the directions  $\theta$ , and  $\mathbf{r}_{\theta}^k$  are the right eigenvectors of the matrix  $M^*$  for each value of  $\theta$ . In order to solve for the unknowns, use is also made of the left eigenvectors of that matrix

$$\mathbf{l}_{\theta}^{1} = \begin{pmatrix} \frac{1}{2} \\ \frac{c}{2g} cos\theta \\ \frac{c}{2g} sin\theta \end{pmatrix}, \ \mathbf{l}_{\theta}^{2} = \begin{pmatrix} \frac{1}{2} \\ -\frac{c}{2g} cos\theta \\ -\frac{c}{2g} sin\theta \end{pmatrix}, \ \mathbf{l}_{\theta}^{3} = \begin{pmatrix} 0 \\ -sin\theta \\ cos\theta \end{pmatrix}$$
(4.16)

and of the unit vector normal to  $\mathbf{n}_{\theta}$ 

$$\mathbf{s}_{\theta} = (-\sin\theta, \cos\theta).$$

Multiplication of (4.16) on the left by  $\mathbf{l}_{\theta 1}^1$  and the left projection over  $\mathbf{s}_{\theta 2}$  gives

$$\mathbf{s}_{\theta 2}.(\mathbf{l}_{\theta 1}^{1}.\nabla\mathbf{V}) = \alpha_{\theta 1}^{1}(\mathbf{s}_{\theta 2}.\mathbf{n}_{\theta 1}), \tag{4.17}$$

where the property  $\mathbf{l}_{\theta}^{i} \cdot \mathbf{r}_{\theta}^{j} = \delta_{ij}$  and the orthogonality between vectors **s** and **n** 

have been used.

From (4.17), we obtain,

$$\alpha_{\theta 1}^{1} = -\frac{\mathbf{s}_{\theta 2} \cdot (\mathbf{l}_{\theta 1}^{1} \cdot \nabla \mathbf{V})}{\sin(\theta_{2} - \theta_{1})}.$$
(4.18)

In case the above notation may be rather obscure, the vector products contained can be developed as

$$\alpha_{\theta 1}^{1} = -\frac{1}{\sin(\theta_{2} - \theta_{1})} \left[ (-\sin\theta_{2}, \cos\theta_{2}) \frac{1}{2} \begin{pmatrix} h_{x} + \frac{c}{g} \cos\theta_{1} u_{x} + \frac{c}{g} \sin\theta_{1} v_{x} \\ h_{y} + \frac{c}{g} \cos\theta_{1} u_{y} + \frac{c}{g} \sin\theta_{1} v_{y} \end{pmatrix} \right].$$

In that way, the six unknowns of the problem are given by

$$\alpha_{\theta 1}^{k} = -\frac{\mathbf{s}_{\theta 2} \cdot (\mathbf{l}_{\theta 1}^{k} \cdot \nabla \mathbf{V})}{\sin(\theta_{2} - \theta_{1})} , \quad \alpha_{\theta 2}^{k} = \frac{\mathbf{s}_{\theta 1} \cdot (\mathbf{l}_{\theta 2}^{1} \cdot \nabla \mathbf{V})}{\sin(\theta_{2} - \theta_{1})}. \tag{4.19}$$

As an illustration, in the particular case of choosing as propagation angles,  $\theta_1 = 0, \theta_2 = \pi/2$ ,

$$\alpha_{\theta 1}^{1} = \frac{1}{2}(h_x + \frac{c}{g}u_x)$$

$$\alpha_{\theta 1}^{2} = \frac{1}{2}(h_x - \frac{c}{g}u_x)$$

$$\alpha_{\theta 1}^{3} = v_x$$

$$\alpha_{\theta 2}^{1} = \frac{1}{2}(h_y + \frac{c}{g}v_y)$$

$$\alpha_{\theta 2}^{2} = \frac{1}{2}(h_y - \frac{c}{g}v_y)$$

$$\alpha_{\theta 2}^{3} = -u_y.$$

#### 4.3 Mach-angle splitting

One of the options proposed within Rudgyard's wave models is the particular choice of the angles that satisfy the equation

$$\mathbf{u.n} - c = 0,\tag{4.20}$$

that is, those angles that make the velocity of one of the acoustic waves vanish. They are obtained from algebraic manipulation of (4.20) and can be expressed as

$$\theta_{1} = \arctan\left(\frac{v + u\sqrt{(M^{2} - 1)}}{u - v\sqrt{(M^{2} - 1)}}\right)$$

$$\theta_{2} = \arctan\left(\frac{v - u\sqrt{(M^{2} - 1)}}{u + v\sqrt{(M^{2} - 1)}}\right)$$
(4.21)

with  $M^2 = \frac{u^2 + v^2}{c^2}$  representing the Froude number in this case. This technique gives very good results in gasdynamics problems for supersonic flows but is not directly applicable to the subsonic case. It can nevertheless be adapted for subsonic (subcritical in our case) flows by replacing  $M^2 - 1$  with  $\max(|M^2 - 1|, \epsilon)$ , the tolerance  $\epsilon$  taking a typical value of 0.1.

#### 5 Numerical Results

The treatment of the solution at the points on the boundaries of the domain has been kept as close as possible to the theory of characteristics in 2D. In all cases, the number of physical conditions to be imposed has been determined by this theory. This number is defined [6] by the signs of the eigenvalues  $\lambda$  of the matrix

$$K = An_x + Bn_y (5.1)$$

where the boundary normal vector  $\mathbf{n}$  is the unit vector pointing into the domain. The eigenvalues are associated with the celerities of the waves. Hence, when  $\lambda$  is positive, the information travels along the normal, into the domain. When it is negative, the information goes against the normal, that is out of the domain. The subcritical cases are the most illustrative, having, at a subcritical inlet for instance,  $\mathbf{u} \cdot \mathbf{n} > 0$  and  $\mathbf{u} \cdot \mathbf{n} < c$ , so that,

$$\lambda_1 = \mathbf{u} \cdot \mathbf{n} < 0$$

$$\lambda_2 = \mathbf{u} \cdot \mathbf{n} + c > 0$$

$$\lambda_3 = \mathbf{u} \cdot \mathbf{n} - c < 0.$$

This means that there are two waves from outside and therefore, two boundary conditions have to be imposed. The wave from inside produces a numerical boundary condition. In an analogous manner, the case of a subcritical outlet requires only one imposed external boundary condition. The information that travels from inside the domain is determined by the compatibility relations which can be written for arbitrary propagation directions from the 2D theory of characteristics. These have been simplified by assuming that the derivatives along the direction tangential to the boundary are negligible. In the case of a material wall boundary, a zero normal velocity is imposed and the depth as well as tangential velocity are calculated from the compatibility conditions.

For the interior points we used the non-linear PSI advection algorithm [10] for all the test cases following but obtained very similar results with the other advection schemes. As for the wave model, the calculations correspond to Rudgyard's decomposition having been found more robust, in general, than the one corresponding to Roe's model D.

#### 5.1 Oblique hydraulic jump

With numerical schemes it is highly desirable to be able to check their predictions against suitable test problems, preferably ones for which an exact solution is available. Such is the case for the example below, computed by a finite volume method by Alcrudo and Garcia-Navarro [1], in which an oblique hydraulic jump is induced by means of the interaction between a supercritical flow and a wall at an angle  $\theta$ . The equation for the angle formed by the shock wave, is defined by

$$\sin\beta = \frac{1}{Fr_1} \sqrt{\frac{h_2}{2h_1} (\frac{h_2}{h_1} + 1)}.$$
 (5.2)

A 2400 element triangular mesh was used to reproduce the discontinuous flow in a case where  $\theta = 8.95^{\circ}$ . The initial conditions were h = 1m, u = 8.57m/s and v = 0m/s, that is, a uniform supercritical flow with Fr = 2.74. Supercritical flow boundary conditions were applied both upstream and downstream. This means that all the variables were specified in the former and all of them updated from interior points in the latter.

The exact solution corresponding to the upstream flow and geometry imposed was calculated. The predicted values were  $h_2 = 1.5$ m,  $|u_2| = 7.9556$ ,  $Fr_2 = 2.075$  for the downstream variables and  $\beta = 30^{\circ}$  for the angle of the jump connecting them to the given upstream conditions. As can be seen in Fig. 1, the agreement of the numerical results with the correct solution was very good. The angle formed by the well defined oblique hydraulic jump is closely reproduced as well as the values of the flow variables on both sides of it  $(h_2 = 1.5049$ m,  $|u_2| = 7.9419$ ,  $Fr_2 = 2.068$ ) and a discontinuous water surface devoid of oscillations is obtained.

The same degree of accuracy is achieved on the mesh with both fluctuation splitting and the TVD in finite volume method reported in [1], but at a higher computational cost in the case of the former technique (a factor of about five). A strategy of cell movement proposed by Baines [5] can be nevertheless exploited for the unstructured grid in order to overcome this difficulty. The possibility of using an algorithm capable of making the cells migrate towards the regions of steeper gradients allows the reduction of the total number of cells. A preliminary, but encouraging, result is displayed in Figs. 2-4. Fig.2 shows the 96 element grid that has been automatically rearranged according to the evolution towards the steady state of the flow, Fig.3. The accuracy of the result displayed in Fig.4 is superior and the computational time has been reduced to half of that used by the TVD method.

# 5.2 Unsteady flow in a converging-diverging sloping channel

In order to test the performance of the multi-dimensional upwinding when including source terms in the system of equations, a simulation of a dambreak wave in a 2D laboratory experiment, as reported in [3], is presented. At the same time,

and unlike in the case of the Euler equations, most practical problems involving the shallow water equations are time-dependent, so this problem also tests the temporal accuracy of the method. The treatment of the source terms was done simply by calculation of the functions at the vertices of every cell, including these values in the updating at every time level, that is, in a pointwise manner.

The channel is 21m long and 1.4m wide at it widest part. It has a uniform bottom slope  $S_{0x}$  along the direction of the main flow. The roughness of the surface (smooth steel-glass) is represented by a Manning's coefficient n = 0.012. Measured data of the water levels as a function of time were available at five positions along the centreline of the flume. The points of measurement are shown in Fig. 5

A dam is placed in the constriction, at x=8.5m from the origin, where the width is 0.6m. The discontinuous initial conditions consist of a horizontal surface level on the upstream side, with a depth of 0.3m just behind the dam, and a uniform water depth downstream. All velocities are initially set equal to zero. The lateral and upstream boundaries are treated as closed walls. The downstream side was treated as a supercritical boundary in the sense of not applying any particular external boundary condition but calculating the values of the variables from the normal updating at the vertices.

The validation of the method was done on a 672 element triangular grid. The case of dambreak flood wave propagation over an initial water depth  $h_2 = 0.053$ m and zero bottom slope is displayed in Figs. 6-9. The results from the calculation are plotted as a solid line and the circles represent the measured data. The solid lines follow closely the experimental results. Apart from downstream boundary effects, the wave front celerity and intensity are well reproduced by the model, as indicated by the rising parts of the curve in Figs. 8 and 9. The good agreement deteriorates, however, when the moving reflected wave is met. The use of a boundary condition different from the weir-type is responsible for this circumstance which is independent of the scheme used in the interior and also happens with other numerical solutions, as reported in [9].

Dry bed initial conditions downstream of the dam corresponding to a bottom slope  $S_{0x} = 0.01$  were also tried. The set of results is plotted in Figs. 10-13. The overall quality of the results is as good as those obtained with a high order finite volume method [3], [9].

#### 6 Conclusions

Two dimensional wave decomposition and multi-dimensional upwinding seem a promising method of solution for the 2D shallow water equations. Two wave models have been adapted to render the technique suited to hydraulic problems with shocks. As with the 1D TVD schemes, our experience with using the multi-dimensional upwind approach for the shallow water equations has closely

followed that of the researchers solving the Euler equations (with both the advection schemes and wave models) showing the same properties as for that system of equations.

Although the procedure is more complicated and costly than present day generalizations of 1D upwinding techniques it is based on a triangular discretization and, by taking advantage of the triangles, the disadvantages can be overcome making the schemes very competitive, and the future for them then looks much more promising. They can clearly be applied to arbitrary geometries, a great advantage for hydraulic engineers working on practical problems, and there is a wide variety of possibilities concerning grid movement and adaption.

### 7 Acknowledgment

We would like to thank Dr. Mike Baines for many useful and interesting discussions during the course of this work.

#### References

- [1] Alcrudo, F. and Garcia-Navarro, P., "A high-resolution Godunov-type scheme in finite volumes for the 2D shallow-water equations" Int. J. of Numerical Methods in Fluids, 16, pp. 489-505 1993.
- [2] Baines, M. "Algorithms for optimal discontinuous piecewise linear and constant L<sub>2</sub> fits to continuous functions with adjustable nodes in 1 and 2 dimensions" to appear in Math. Comp., April1994.
- [3] Bellos, C.V., Soulis, J.V. and Sakkas, J.G., "Computation of two-dimensional dam-break induced flows." Adv. Water Resources, 14, pp. 31-41, 1991.
- [4] Cunge, J.A., Holly, F.M. and Verwey, A., "Practical Aspects of Computational River Hydraulics." Pitman Pub. Inc, 1980.
- [5] Deconinck, H., Struijs, R., Bourgois, G., Paillere, H. and Roe, P.L., "Multi-dimensional Upwind Methods for Unstructured Grids." In Unstructured Grid Methods for Advection Dominated Flows, May 1992, AGARD 787.
- [6] Hirsch, Ch., "Numerical Computation of Internal and External Flows, Vol.2: Computational Methods for Inviscid and Viscous Flows" Wiley, Chichester, 1990.
- [7] Fennema, R.J., and Chaudhry, M.H., "Explicit methods for 2D transient free surface flows" J. of Hydraulic Engineering, ASCE, 116, pp. 1013-1034, 1990.
- [8] Garcia-Navarro, P., and Alcrudo, F., "1D Open Channel Flow Simulation Using TVD McCormack Scheme" J. of Hydraulic Engineering, ASCE, 118, pp. 1359-1373, 1992.

- [9] Garcia-Navarro, P. and Alcrudo, F., "A TVD scheme in finite volumes for the simulation of 2D discontinuous flows" Proceedings of the XXV IAHR Congress, Tokyo 1993.
- [10] Hubbard, M.E., "A Survey of Genuinely Multidimensional Upwinding Techniques." Numerical Analysis Report, 7/93, Department of Mathematics, University of Reading, UK. 1993.
- [11] Roe, P.L., "Discrete Models for the Numerical Analysis of Time-Dependent Multidimensional Gas Dynamics." Journal of Computational Physics, 63, pp. 458-476, 1986.
- [12] Roe, P.L., "A Basis for Upwind Differencing of the Two-Dimensional Unsteady Euler Equations." Numerical Methods for Fluid Dynamics II, K.W.Morton and M.J.Baines editors, pp. 55-80, Oxford University Press, 1986.
- [13] Roe, P.L., Struijs, R. and Deconinck, H., "A Conservative Linearisation of the Multidimensional Euler Equations." Journal of Computational Physics, to appear.
- [14] Rudgyard, M., "Multidimensional Wave Decompositions for the Euler Equations." VKI Lecture Series, 'Computational Fluid Dynamics', 1993.
- [15] Struijs, R., Roe, P.L. and Deconinck, H., "Fluctuation Splitting Schemes for the 2D Euler Equations." VKI Lecture Series 1991-01, 'Computational Fluid Dynamics', 1991.

## List of Figures

1	Map of level lines from the numerical result obtained in the 2400	0.1
	elements grid	21
2	96 elements initial grid used for the oblique jump test case	21
3	Above: 96 elements distorted grid used for the oblique jump test	
	case	22
4	Map of level lines from the numerical result obtained in the 96	
	elements distorted grid	22
5	Unsteady flow through a converging diverging channel. Geometry	
	and points of measurement	23
6	Test case $S_{0x} = 0.0$ , $h_1 = 0.3$ m, $h_2 = 0.053$ m. Continuous line: Pre-	
	dicted values. Circles: Measured values. Section 2	24
7	Test case $S_{0x} = 0.0$ , $h_1 = 0.3$ m, $h_2 = 0.053$ m. Continuous line: Pre-	
	dicted values. Circles: Measured values. Section 3	24
8	Test case $S_{0x} = 0.0$ , $h_1 = 0.3$ m, $h_2 = 0.053$ m. Continuous line: Pre-	
	dicted values. Circles: Measured values. Section 5	25
9	Test case $S_{0x} = 0.0$ , $h_1 = 0.3$ m, $h_2 = 0.053$ m. Continuous line: Pre-	
	dicted values. Circles: Measured values. Section 6	25
10	Test case $S_{0x} = 0.01$ , $h_1 = 0.3$ m, $h_2 = 0.0$ m. Continuous line: Pre-	
	dicted values. Circles: Measured values. Section 2	26
11	Test case $S_{0x} = 0.01$ , $h_1 = 0.3$ m, $h_2 = 0.0$ m. Continuous line: Pre-	
	dicted values. Circles: Measured values. Section 3	26
12	Test case $S_{0x} = 0.01$ , $h_1 = 0.3$ m, $h_2 = 0.0$ m. Continuous line: Pre-	
	dicted values. Circles: Measured values. Section 5	27
13	Test case $S_{0x} = 0.01$ , $h_1 = 0.3$ m, $h_2 = 0.0$ m. Continuous line: Pre-	
	dicted values. Circles: Measured values. Section 6	27

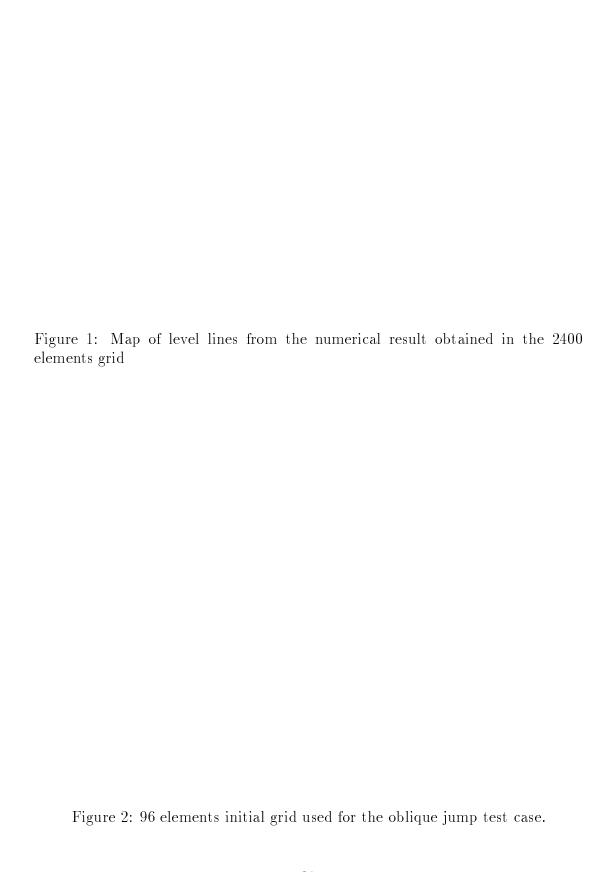




Figure 5: Unsteady flow through a converging diverging channel. Geometry and points of measurement

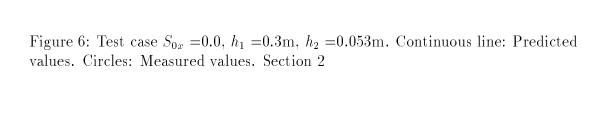


Figure 7: Test case  $S_{0x}=0.0,\ h_1=0.3\mathrm{m},\ h_2=0.053\mathrm{m}.$  Continuous line: Predicted values. Circles: Measured values. Section 3

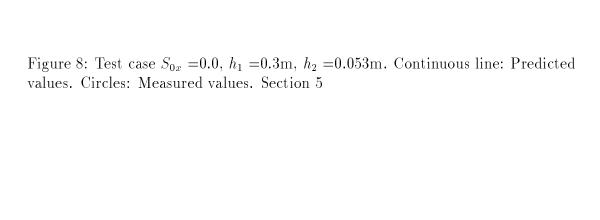


Figure 10: Test case  $S_{0x}=0.01,\ h_1=0.3\mathrm{m},\ h_2=0.0\mathrm{m}.$  Continuous line: Predicted values. Circles: Measured values. Section 2

Figure 11: Test case  $S_{0x}=0.01,\ h_1=0.3\mathrm{m},\ h_2=0.0\mathrm{m}.$  Continuous line: Predicted values. Circles: Measured values. Section 3

Figure 12: Test case  $S_{0x}=0.01$ ,  $h_1=0.3$ m,  $h_2=0.0$ m. Continuous line: Predicted values. Circles: Measured values. Section 5

Figure 13: Test case  $S_{0x}=0.01,\ h_1=0.3\mathrm{m},\ h_2=0.0\mathrm{m}.$  Continuous line: Predicted values. Circles: Measured values. Section 6